On the Measurement and Prediction of the Out-of-Plane Displacement Surrounding Cold-Expanded Holes

L. D'Acquisto · S. Pasta

Abstract Experimental measurements of the out-of-plane displacement surrounding cold-expanded holes in a 6082-T6 aluminum alloy were made with a 3D optical scanner using the technique of the encoded light-pattern projection in white light. The measured surface profiles have shown the thickness discontinuity along the hole edge due to the effect of the split in the sleeve. An analytical–numerical solution of the out-of-plane displacement is presented based on existing analytical models. Thus, the results given by the analytical model were then compared with the experimental data and with a finite element (FE) model that simulates the cold-expansion process. The location of the elastic–plastic boundary was estimated as the point at which no change in thickness was observed; a good agreement was found in the comparison of measured, FE and analytical results. The measured surface profiles agreed with those predicted by the FE model and analytical solution. The proposed experimental approach can be used together with FE analysis for predicting the radial and circumferential residual stresses in cold-expanded hole. It is quite versatile and can also be used as quality-control technique in the manufacturing processes of cold-expanded holes.

Nomenclature

a	Radius of the hole
b	Outside radius of the plate
p	Internal pressure
r	Radius at any points
R	Level of plastic anisotropy
E	Elastic modulus
E_s	Secant modulus
σ	Effective stress
ε	Strain
n	Strain hardening exponent
α	Boudiansky's parameter
$v_{z(r)}^{pl}$	Out-of-plane displacement

Subscripts

r	Refers to the radial direction
θ	Refers to the circumferential direction
z	Refers to the axial direction
a	Refers to the hole edge
p	Refers to the elastic–plastic boundary
y	Refers to initial yielding

Superscripts

pl	Refers to the plastic domain

Introduction

The presence of a fastener hole in a loaded structural component introduces a limiting effect on the fatigue life because of the stress concentration at the hole edge. In order to minimize the detrimental effect of stress concentration, it has been a practice for over 25 years to pre-stress fastener holes by a cold-working process prior to the installation of bolts or rivets. This technique introduces

L. D'Acquisto · S. Pasta (✉)
Department of Mechanics, University of Palermo,
Viale delle Scienze,
90128 Palermo, Italy
e-mail: spasta@dima.unipa.it

compressive residual stresses into the annular region around the hole. The effect of residual stresses is to inhibits the nucleation and growth of cracks arising from hole edge.

The most widely used technique to generate these compressive residual stresses is the split-sleeve cold-expansion process marketed by *Fatigue Technology Inc.*, *FTI*, [1]. In this process, the residual stresses result from the redistribution of stresses following the local plastic deformation of the material close to the hole edge, Fig. 1. A stainless-steel split sleeve is placed over a tapered mandrel that represents the element that transmits pressure. The mandrel and split sleeve assembly is then inserted into the hole to be expanded. The mandrel is drawn back through the hole with the split sleeve held in the hole by the nosepiece of the mandrel puller. The interference due to the major diameter of the mandrel induces a plastic deformation of the material adjacent the hole. When the mandrel is removed and the pressure on the hole is cancelled, a residual stress zone is created due to action of the elastically deformed material on that which has undergone a plastic deformation. The residual stress field is asymmetrical around the hole due to extensive shear deformation caused by the split of the sleeve. It varies significantly through the thickness of the plate as a result of the non uniform deformation produced during the cold expansion, owing to different mechanical constraint at different depths [2].

The literature presents several representative theories to evaluate the residual stress field, and these analytical models are perhaps an example of the historical development of plasticity theory [3–7]. However, these solutions are based on assumptions that neglect the through-thickness changes of residual stresses along the hole bore. Nadai [3] first considered a mandrel as an elastic–plastic deformable tube to be fitted into a drilled plate with the assumptions of elastic perfectly-plastic material model, plane stress condition, and Von Mises yield criterion. A more complicated model is that proposed by Guo [3] which assumes non-linear strain hardening material obeying the modified Ramberg model. Fatigue crack growth tests coupled with AFGROW analyses [8] have shown that the fatigue life for
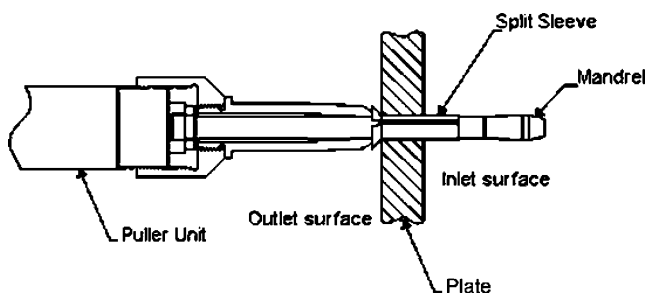
cold-worked holes is improved respect to a plain hole, and that the material mechanical properties, such as the yield stress, strain hardening in tension and compression, can significantly affect fatigue life. With concern to FE simulations, different researchers [9–11] focused on modeling the residual stress field using numerical two-dimensional (2D) or three-dimensional (3D) analyses. One of these [10] highlighted that the residual stress distribution is not uniform across the thickness being the magnitude of residual stresses close to the mandrel outlet face greater than those of the mandrel entrance face. Moreover, a recent analysis [12] highlighted that at pip location corresponding to the split of the sleeve, the hoop residual stress is significantly lower than that at 90° from the pip. Among the experimental techniques, Sach's boring out technique was used by Ozdemir et al. [13] to measure the 3D residual stress distribution around cold-expanded holes. In a most recent publication, Zhang et al. [14] used the innovative contour method described by Prime et al. [15] to obtain 2D maps of residual stresses that they compared with those obtained by 3D finite element simulations. The non-destructive X-ray technique is widely used to determine residual stresses around the expanded hole [2, 16, 17]. Surface measurements or measurements with up to 50 μm of penetration can be made by the X-ray diffraction method, that is also able to predict the reverse yielding zone of cold-expanded holes [18, 19]. Sanford and Link [20] first used the holographic interferometry as an optical method to measure the elastic–plastic boundary on the entrance side of cold-expanded plates. The fringe pattern obtained from the reconstructed hologram was used to determine the position of plastic radius; they compared the experimental results with theoretical predictions of the elastic–plastic boundary. On the basis of this work, Cirello and Pasta [21] used the digital image correlation and digital speckle pattern interferometry techniques to monitor the radial displacement during cold-expansion process and compare it with the analytical solution. They had shown that digital image correlation is more accurate in measuring the radial displacements in the plastic domain whereas digital speckle pattern interferometry performs better in the elastic domain. Poolsuk et al. [22] quantified the elastic–plastic boundary by measuring the change in thickness of the plate by means of a linear variable differential transformer (LVDT). The point at which the surface profiles started to differ indicated an increase in thickness, and was considered as the elastic–plastic boundary. However, this approach was not sensitive enough to evaluate the elastic–plastic boundary if compared with the analytical prediction.

Observing the three-dimensional nature of the cold-expansion process occurring incrementally through the thickness, it is interesting to measure the out-of-plane displacement due to the considerable compression applied

Fig. 1 Sketch of the split-sleeve cold-expansion process developed by FTI; the oversized mandrel is pulled back through the fastener hole

on the surrounding material as the mandrel is pulled through the hole. Therefore, on the base of the Guo's analytical model, a solution is initially presented in this paper to compute the out-of-plane displacement occurring in the plastic domain. Then, it is illustrated the testing procedure makes use of an optical scanner to perform extremely accurate measurements of the out-of-plane displacements surrounding cold-expanded holes along several profiles from the inlet and outlet faces. These measurement were performed on 6082-T6 aluminum plates with thicknesses of 3 mm and 5 mm. Results obtained show even the discontinuity due to the split in the sleeve. These profiles were compared both with those calculated by the numerical solution and with those provided by a FE model simulating the entire cold-expansion process.

The position of the elastic–plastic boundary was also determined from the profiles measured along the surfaces; this parameter can be used to control the interference level of the cold expansion process. Finally, a comparison between analytical and FE circumferential residual stresses has been presented. Although the stresses obtained with the proposed solution were not directly derived from the measured displacements, they could be used to tune the FE model up to a correspondence between measured and calculated out-of-plane displacements.

Analytical Model

The aim of the analytical–numerical model is to provide a computational tool for determining the thickness changes in cold-expanded holes to be compared with those measured by the optical technique. This solution presents drawbacks similar to those of Guo's analytical model [4]; it neglects the asymmetry in the stress state originated by the presence of the split-sleeve and does not take into account the change in stress field along the thickness of the plate.

It is assumed that a hole in a finite circular plate with inner radius, a, and outer radius, b, is subjected to an internal pressure, p. This pressure plasticizes the material up to a plastic radius r_p, as shown in Fig. 2. The relationships of the plastic strains and the stresses, considering the anisotropy caused by plastic flow in the plastic domain ($a < r \leq r_p$), are [5]:

$$
\begin{aligned}
\varepsilon_r^{pl} &= \left(\frac{1}{E_s} - \frac{1}{E}\right)\left(\sigma_r^{pl} - \frac{R}{1+R}\sigma_\theta^{pl}\right) \\
\varepsilon_\theta^{pl} &= \left(\frac{1}{E_s} - \frac{1}{E}\right)\left(\sigma_\theta^{pl} - \frac{R}{1+R}\sigma_r^{pl}\right)
\end{aligned}
\tag{1}
$$

In equation (1), the level of plastic anisotropy is described by R, defined as the ratio of the in-plane transverse plastic strain to the through-thickness plastic
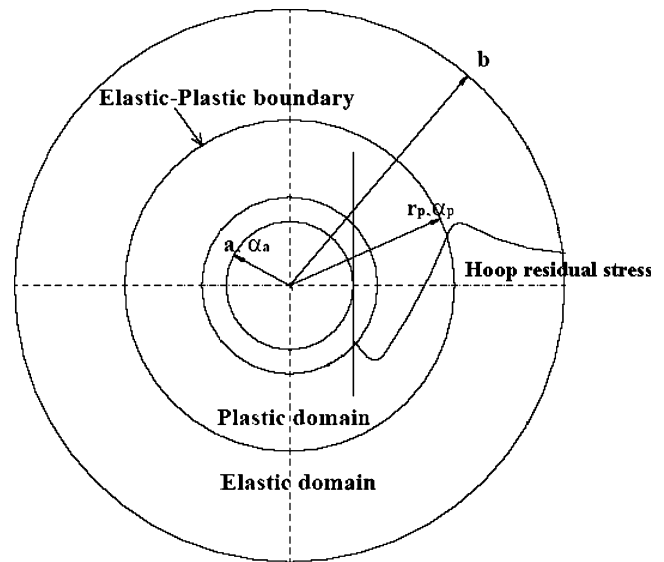

Fig. 2 Schematic of residual stress distribution surrounds a hole in a disk subjected to radial expansion

strain, where $R = 1$ results in isotropic behavior. E_s is the secant modulus at the point σ, ε on the uniaxial stress–strain curve obtained from modified Ramberg model [23]:

$$
\frac{1}{E_s} = \frac{\varepsilon}{\sigma} = \frac{1}{E}\left[\frac{\sigma}{\sigma_y}\right]^{n-1}
\tag{2}
$$

where: n is the strain hardening exponent and σ_y is the yield stress.

Assuming the invariance of the volume of material during cold-expansion process, the following relationship between strains along the three principal directions can be obtained:

$$
\varepsilon_r^{pl} + \varepsilon_\theta^{pl} + \varepsilon_z^{pl} = 0
\tag{3}
$$

Combining equations (1) and (3), the out-of-plane strain, ε_z^{pl}, can be found as function of radial and circumferential stresses:

$$
\varepsilon_{z(r)}^{pl} = \left(\frac{1}{E_s} - \frac{1}{E}\right)\left[\left(\sigma_{r(r)}^{pl} + \sigma_{\theta(r)}^{pl}\right)\left(1 - \frac{R}{1+R}\right)\right]
\tag{4}
$$

Furthermore, the out-of-plane strain is related to the out-of-plane displacement by the following expression:

$$
\varepsilon_{z(r)}^{pl} = \frac{dv_{z(r)}^{pl}}{dz_{(r)}}
\tag{5}
$$

Therefore, the out-of-plane displacements, $v_{z(r)}^{pl}$, can be obtained integrating the equation (5) with the aid of the equation (4) in the plastic domain ($a < r \leq r_p$):

$$
v_{z(r)}^{pl} = \int_a^{r_p} \left(\frac{1}{E_s} - \frac{1}{E}\right)\left[\left(\sigma_{r(r)}^{pl} + \sigma_{\theta(r)}^{pl}\right)\left(1 - \frac{R}{1+R}\right)\right] dz_{(r)}
\tag{6}
$$

The solution of equation (6) is quite complex since the closed-form solution of radial and circumferential stresses was found in terms of Budiansky's parameter $\alpha_{(r)}$ [24], which changes monotonically between the values at the hole edge, α_a, and at the elastic–plastic boundary, α_p. First, a set of transcendental equations (see Appendix) is necessary to compute the plastic radius, r_p, and α_a, and α_p terms. Thus, the radial and circumferential stresses can be determined at any radius value, r, in the plastic domain. Table 1 shows the material parameters experimentally determined for the 6082-T6 aluminum alloy.

The plastic domain was divided into a discrete number of radius increment Δr, so that a discrete value of the out-of-plane displacements can be found by numerical integration of the expression in equation (6). The resulting step distribution converges to the exact solution of $v_{z(r)}^{pl}$ as the size of Δr tends to zero.

The Measurement of Out-of-Plane Displacement

The *FTI* cold-expansion process [1] was used in this investigation to expand up to 4% nominal interference two 6082-T6 aluminum plates having thicknesses of 3 mm and 5 mm. The yield stress (σ_y=255 MPa) and elastic modulus (E=68000 MPa) were experimentally evaluated through a set of tensile specimens. The ASTM E 646-00 test method [25] was used to obtain the strain-hardening exponent (n=17.1) used for both Finite Element simulation and analytical solution, see equation (2). These parameters were calculated from the mean values of several tensile tests, (see Table 1). The plate geometry is a square (W= 50 mm) having an initial radius of the hole equal to 2.8 mm and final radius after cold working of 2.96 mm; these dimensions will be shown in Figs. 6, 7, 8, 9 and 10 as dashed and solid lines, respectively. The hole dimension after reaming was within the diameter tolerance specified by the *FTI* procedure.

After cold-expansion process of holes, images of both the inlet and outlet faces of plates were acquired with the *COMET5* 3D scanner distributed by Steinbichler [26]. This system uses the sequential projection of binary encoded patterns to project multiple patterns in white light on the blinded plate. Thus, a CCD camera having a 100 mm lens acquires the fringe pattern reflected by the plate and provides a cloud of points representing the

coordinate in the space of the plate. Figure 3 shows the whole setup. The cloud consists of approximately four millions points. The accuracy of the measured out-of-plane displacements, as certified by the VDI 2634 standard [27], is 5 µm together with a z-resolution (parallel to the line-of-sight of the Comet) of 1 µm and a lateral resolution (point-to-point distance) of 50 µm. The highest resolution of the method can be obtained when the cloud of points is focused in the smallest volume of observation ($100\times100\times100$ mm). The baseline shown in Figs. 6, 7, 8, 9 and 10 was obtained by least square fitting of experimental points measured in the plate region sufficiently far-off the cold-expanded zone. The acquisitions were performed at angular steps of 45° of the rotating table holding the blinded plate. Thus, the elaboration algorithm implemented in the 3D system was employed to reconstruct the shape of the cold-worked hole. This software also provides the rotation matrix needed to align the shape of the cold-worked hole to the reference plane of the measurement system. In particular, it has been created a "fictitius" plane on the reconstructed shape for rotating the same shape through the tilt angles provided by the rotation matrix. The cloud was exported in a mesh (stereolitography file) after cleaning and optimization procedures of points. The closest measurement position to the bore of the hole was set to about 0.5 mm in order to avoid edge effects. Edge effects in fact harm the procedure of shape recovery based on the cloud of points provided by the COMET5 measurement
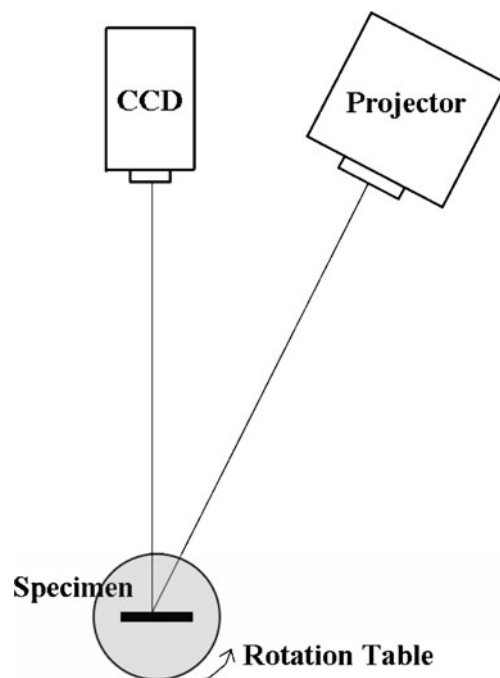
Table 1 Material parameters experimentally determined for the 6082-T6 aluminum alloy and used for theoretical prediction and FE analysis

σ_y [MPa]	E [MPa]	ν	n	R
255	68000	0.3	17.1	1

Fig. 3 Setup of *COMET5* 3D scanner using the encoded light-pattern projection technique for obtaining the shape of cold-worked holes

device. The processing was performed through Rhinoceros® software [28], and the measurements of the out-of-plane displacement were carried out for angular directions corresponding to the split of the sleeve (0° configuration) and every 45° from the split.

Given the symmetry of the problem with respect to the cross section containing the split of the sleeve and the vertical axis of the hole, the 45°, 90°, and 135° configurations are symmetric to those at 315°, 270°, and 225°, respectively; therefore, the arithmetic mean of these data will be presented (i.e. 45°–315°, 90°–270°, and 135°–225°).

Finite Element Simulation

3D numerical analyses were carried out to simulate the entire cold-expansion process with DEFORM-3D™ software [29], a Lagrangian implicit code designed to analyze metal forming processes, that is extremely effective in a wide range of research and industrial applications. The simulations provided the out-of-plane displacement and residual stress field around expanded hole of 3 mm and 5 mm thick plates; then, an experimental–numerical comparison has been carried out to validate the FE model.

All objects of the cold-expansion process were simulated, Fig. 4. The split sleeve and the mandrel have better mechanical properties than the plate has; consequently, the split sleeve was considered elastic, while the mandrel was assumed to be rigid bodies. The material behavior of the plate, implemented both in FE analysis and in Guo's analytical model, was taken into account by means of an elastic–plastic model with a kinematic hardening model fit for the simulation of plastic cold-working, using the Bauschinger's parameter [30]. The elastic data are governed by both E and ν coefficients whereas the plastic-flow behavior in plastic domain obeys to a non-linear stress–strain curve described by n and σ_y parameters (see Table 1). The geometries and dimensions of the mandrel and split sleeve are the same as those of *FTI* cold-expansion process [1]. Tetra elements with four nodes were used for the mesh of the plate and split sleeve. The element size was improved through a finer mesh density close to the hole edge to predict the steep stress gradient that arises there. The plate has been modeled by 123000 elements and the split sleeve by 20000; these numbers were sufficient to ensure accurate representation of the stress field. During the mandrel movement, the remeshing was automatically calculated to conveniently handle the remeshing of objects undergoing large plastic deformation. To simulate the reaction of the nosepiece of the puller, the plate was constrained
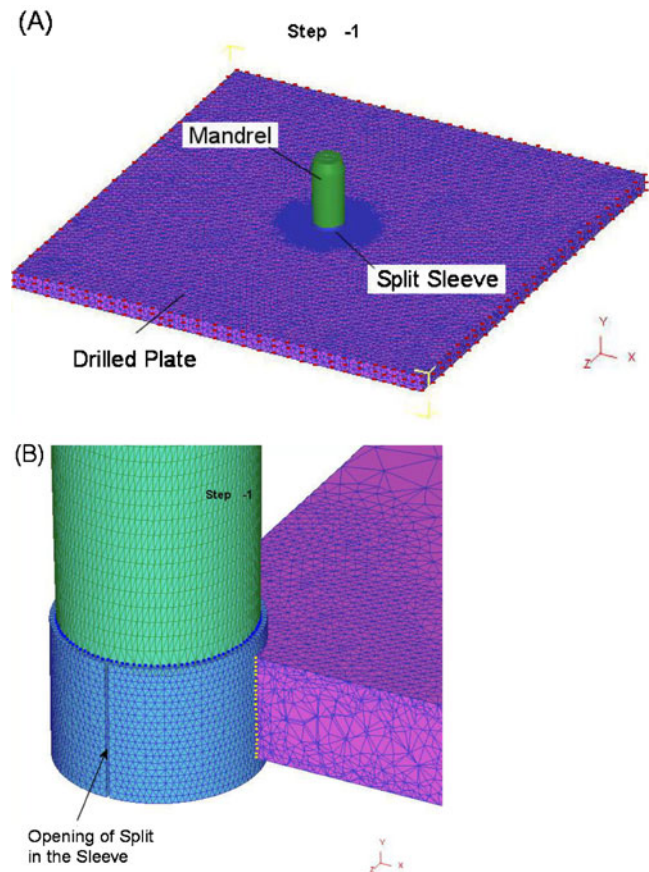

Fig. 4 FE model used to simulate the cold-expansion process of the hole: (a) complete model, (b) detailed view close to hole edge

along the axial direction away from the hole bore, (red dots in Fig. 4(a) indicate this boundary condition for the drilled plate); this does not influence the displacement distribution. The boundary contact conditions among objects (mandrel, split sleeve, and plate) were expressed by means of contact elements; Fig. 4(b) with a detailed view close to hole edge shows the contact conditions between mandrel and split sleeve (blue dots) and split sleeve and plate (yellow dots). During the process, the contact elements are automatically activated. A mandrel speed of 4 mm/s was adopted to simulate the process. The coefficient of friction was assumed to be equal to 0.3, a typical value representing the contact between aluminum and steel under lubricated condition [31]. The loading and unloading steps of the process were simulated with a total of 315 steps of the process with an increment of 0.1 mm mandrel displacement.

At the end of the simulation the finite element mesh was imported into Rhinoceros® environment [28] for further processing and the nodal out-of-plane displacement were compared with experimental ones in the same position.

Results and Discussion

Shape of a Cold-Worked Hole

Image acquisitions performed during experiments by the means of 3D optical scanner provided very accurate shapes of the region surrounding the cold-expanded hole. Figure 5 displays a particular view of the outlet face of the hole after an expansion at the 4% nominal interference in a 3 mm plate. It is worth to observe that the presence of the split in the sleeve does not provide for a uniform expansion of the hole. As the mandrel is being pulled through the hole, a certain amount of material is stretched in the axial direction of the hole, thereby increase in the thickness of both inlet and outlet faces of the cold-expanded hole is observed. However a lower amount of variation of thickness occurs in correspondence of the split in the sleeve especially in the inlet face because a reduced expansion is observed in this region as is shown in Fig. 5.

Measured Out-of-Plane Displacements

Measurements of the out-of-plane displacements were carried out along several angular directions each of which were at 45° from the previous one; the average of the out-of plane displacements was calculated for symmetric profiles as described in "The Measurement of Out-of-Plane Displacement". Figure 6 shows the profiles of the out-of-plane displacement on both inlet and outlet face for the 3 mm thick plate. It can be noticed that the highest values of displacements occur at an angular direction of 45°–315° with respect to the position of the split in the sleeve for both inlet and outlet face of the hole. The lowest out-of-plane displacements were found for both faces at the location of the split in the sleeve (i.e. at 0°), because a lower pressure occurs in this zone during cold expansion process. In addition, out-of-plane displacements at 135°–225° and 180° are lower than those at 45°–315° and 90°–270°. In general,
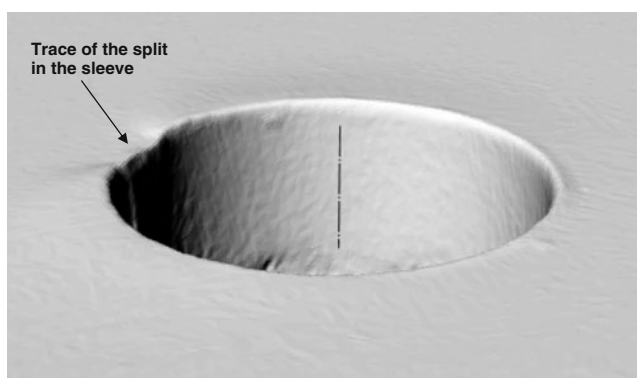

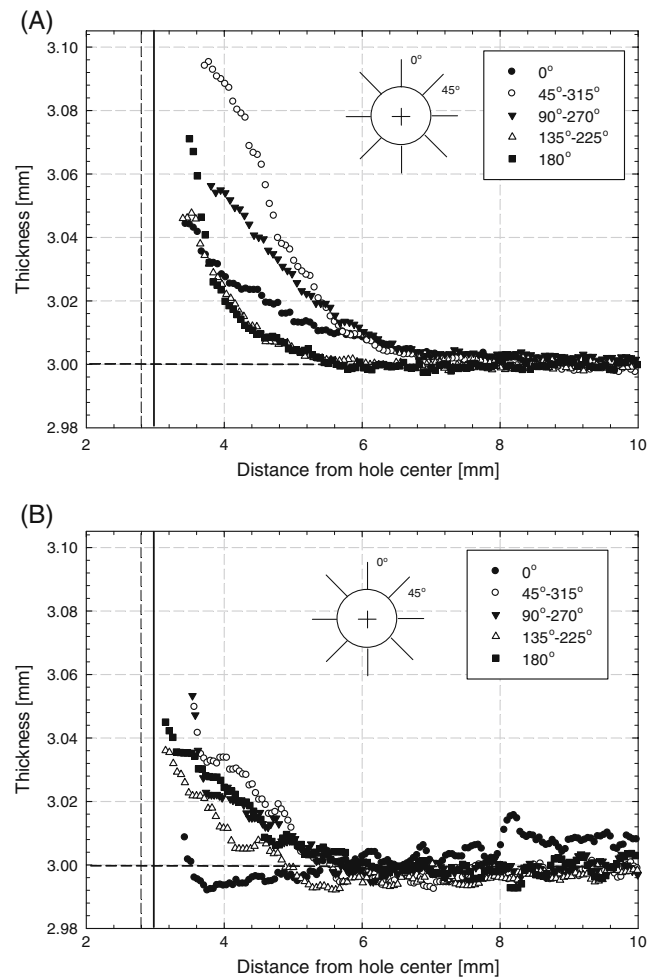**Fig. 5** Shape of the inlet face of cold-expanded hole acquired with *COMET5* 3D scanner for 3 mm thick plate

Fig. 6 Measurements of thickness obtained from 3D optical scanner on (**a**) outlet face and (**b**) inlet face of cold-expanded hole having thickness of 3 mm

the inlet face exhibits out of plane displacements lower than that of the outlet face; this may be due to the axial action of the pulled mandrel that tends to compress the material on the inlet face and to stretch that on the outlet face. The analytical solution of cold-expanded problem asserts that the elastic–plastic boundary occurs when the out-of-plane plastic strain is zero, elastic strain ε_z is constant and therefore the out-of plane displacement is zero. Therefore the plastic radius can be estimated as the point at which no changes in thickness were observed. In the outlet face, the plastic radius occurs at 7.3 mm from hole center whereas the values is considerable lower (r_p=6 mm) in the inlet face. This result is in accordance to the measurements of residual stresses performed by Ozdemir et al. [13]. These changes in the out-of-plane displacement highlight the three-dimensional nature of cold-expansion process and are not considered in the analytical models; consequently, a non-uniform distribution of radial and circumferential stress will occur. Similar measurements of the out-of-plane

displacement were obtained for 5 mm thick plate, Fig. 7. In this case, the magnitudes of the out-of-plane displacement appear slightly lower than those of 3 mm thick plate. An increase in the plate thickness corresponds to a reduction in the out-of-plane displacements. It was clearly observed in the comparison between 5 mm and 3 mm thick plates. A similar reduction in residual stresses for increasing thickness of the plate was also observed in a previous work [12].

Experimental-FE Comparison

The deformed meshes at the post-process stage of the FE simulation of cold-expansion process were used to obtain the out-of-plane displacement profiles as those shown by the experiments. The experimental-FE comparisons were made on the outlet face since it exhibits the higher values of the out-of-plane displacement. Figures 8 and 9 show the displacement profiles for both 3 mm and 5 mm thick plates for each angular direction. Except for the angular direction

corresponding to the position of the split in the sleeve (0° configuration), overall, the FE profiles obtained by simulating the cold-expansion process match with those experimentally obtained from the 3D laser scanner.

The FE results present a steeper transition in out-of plane displacements in the boundary region within plastic and elastic zones, compared to experimental measurements. This may be due to differences in the material parameters, particularly the yielding stress and strain hardening exponent, since the element size was considerably small. The 5 mm thick plate exhibits closer values of the out-of-plane displacement; moreover, it has been observed that the FE and experimental profiles at 45°–315° and 90°–270° overlap each other. The plastic radius obtained from the FE analysis (r_p=7.6 mm) results slightly greater than that of experiments. Therefore the good correspondence of out-of-plane displacement and plastic radius confirms that the FE simulation can be useful to predict the residual stresses in cold expanded holes.

Experimental–Analytical Comparison

Finally the profile of the out-of-plane displacement measured with the 3D optical scanner was compared with that predicted by the analytical solution; in particular, the lowest (0° configuration) and highest (45°–315° configuration) profiles of both 3 mm and 5 mm plates were compared to those predicted by the analytical solution, see Fig. 10. Only marginal agreement can be observed between predicted and measured profiles. In particular, the general trend of data is different except for the peak of 45°–315° configuration of 3 mm thick plate for which the magnitude of the out-of-plane displacement matches with the predicted. In a similar way, the predicted plastic radius, which was found plotting the residual stress of the FE simulation, is approximately 8 mm; this is greater than that of experiments possibly due to the effect of material. One possible explanation may be that the boundary conditions assumed by the theories do not match those of the cold-expansion process. This has been also shown by previous experimental [13] and finite element [9, 12] works that highlight how the predicted residual stresses would have to be compared with those on the outlet face rather than the mid-thickness one. Moreover the three-dimensional nature of the process is strongly affected by the presence of the split sleeve and this fact is not considered in the theories in which the plate thickness does not play any role.

Determination of Stress Field

The evaluation of the circumferential residual stress σ_θ in cold-expanded holes is a relevant issue since this stress affects significantly the fatigue crack growth. In general,
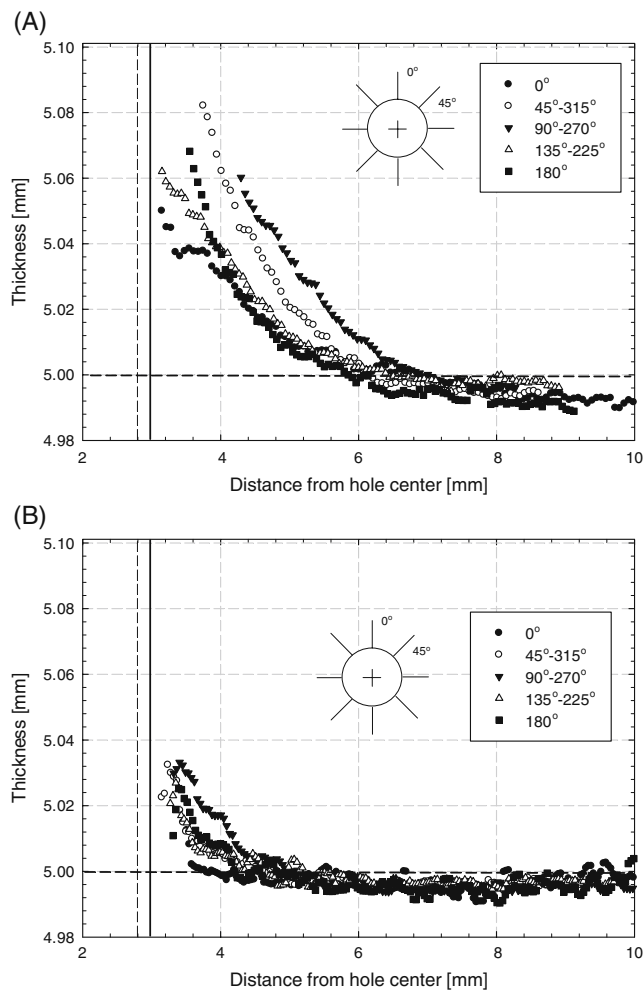
Fig. 7 Measurements of thickness obtained from 3D optical scanner acquisitions on (a) outlet face and (b) inlet face of cold-expanded hole having thickness of 5 mm
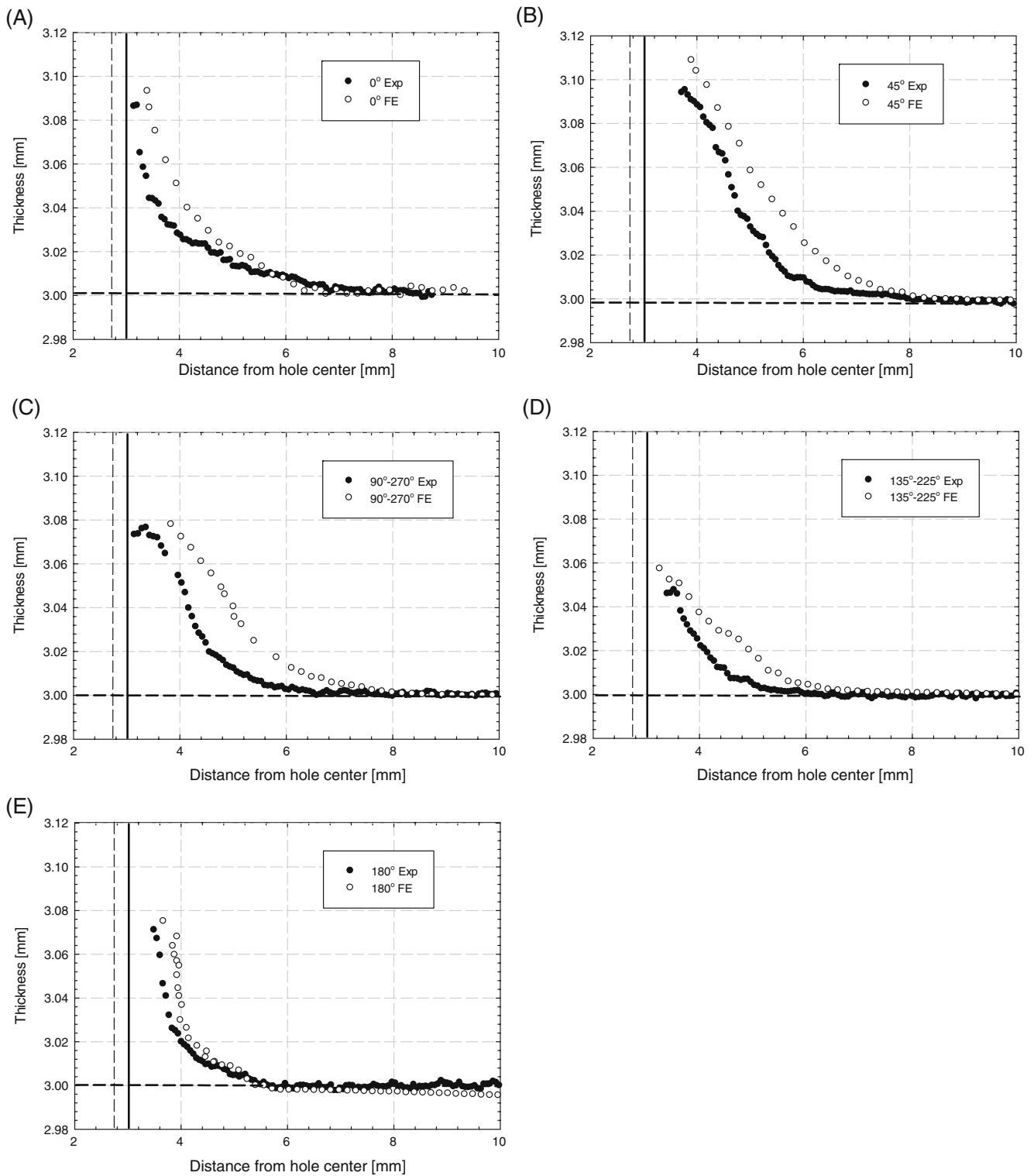
Fig. 8 Experimental-finite element comparison of thickness on outlet face of the 3 mm thick plate

the ε_z strain field can be obtained by deriving the out-of-plane displacements obtained experimentally. However, the obtained ε_z value depends on the sum of both σ_r and σ_θ so that stress separation technique requires additional infor-

mation to be applied, or the assumption to neglect σ_r to get the σ_θ stress directly.

On the basis of the knowledge of the measured out-of-plane displacements field, a FE model of the cold-working
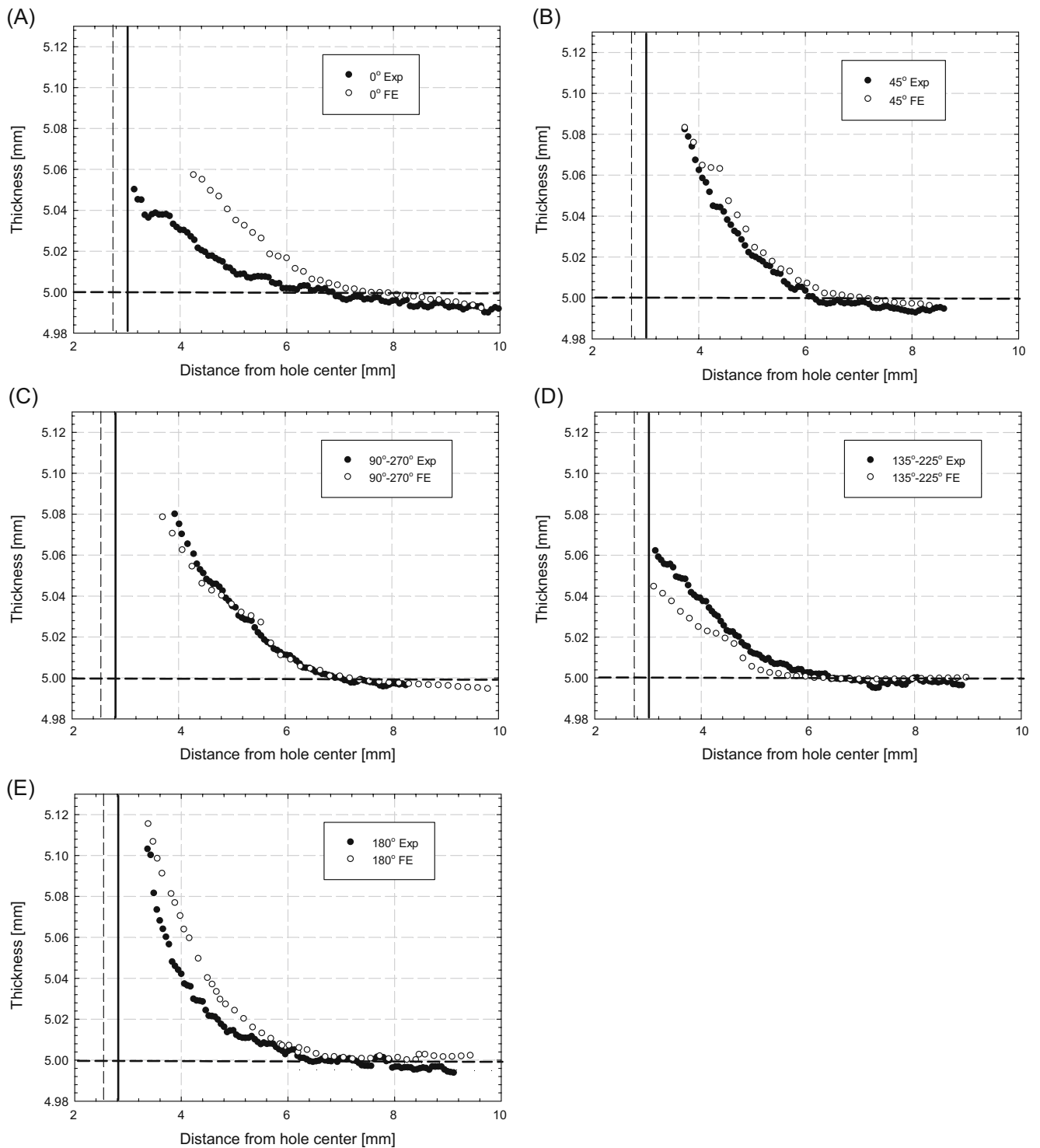
Fig. 9 Experimental-finite element comparison of thickness on outlet face of the 5 mm thick plate

process for the expanded hole can be developed to provide the out-of-plane displacement field that are similar to those measured both at the inlet and outlet faces. This procedure can be refined by properly tuning the material parameters up to a correspondence between measured and calculated out-of-plane displacements. At this point the calculated

circumferential residual stresses can be assumed to be a good prediction of those acting on the real plate. Figure 11 shows a comparison of FE prediction of the circumferential residual stress with Guo's solution, evidencing a good agreement between the numerical simulation and analytical model. In particular, the FE simulation slightly under-
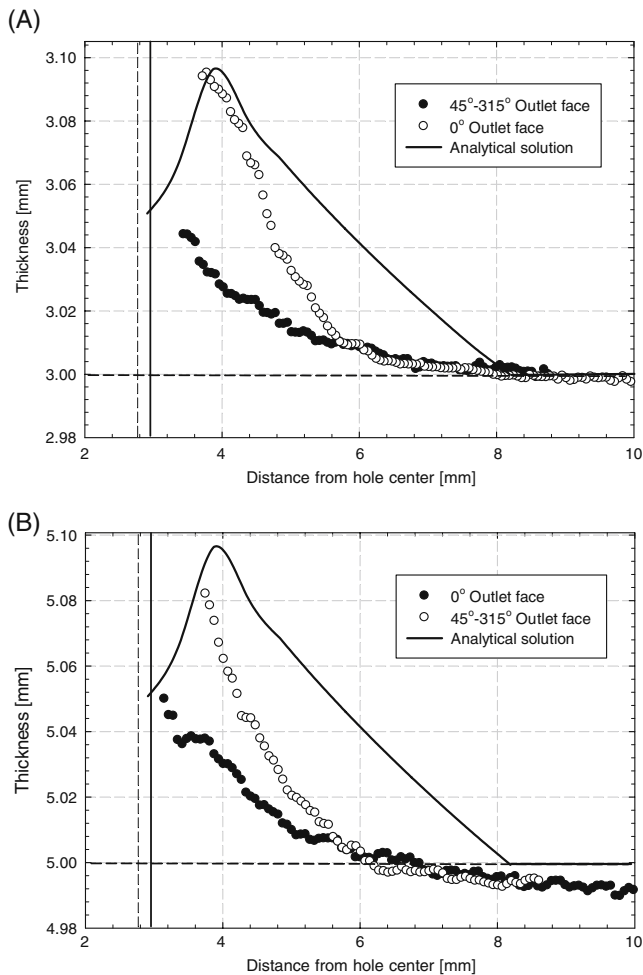
(A)

(B)

Fig. 10 Thickness at 0° and 45°–315° configurations of (**a**) 3 mm and (**b**) 5 mm thick plates compared with analytical prediction
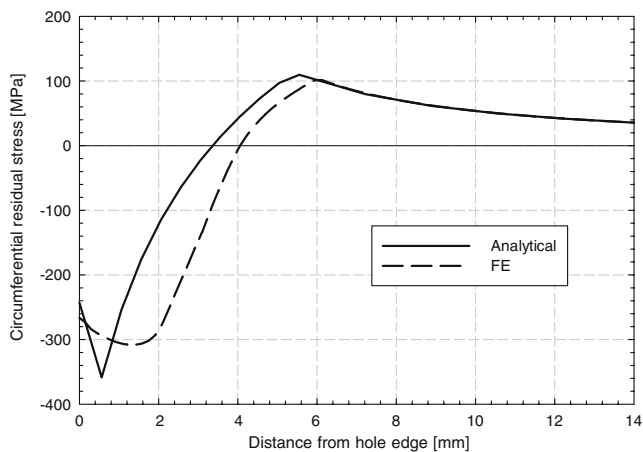

Fig. 11 Comparison of FE hoop residual stress with Guo's solution (3 mm plate)

estimates the maximum and minimum magnitudes of the circumferential residual stress. The reverse and plastic radiuses are in agreement with those provided by the Guo's solution.

Conclusions

The measurements of the out-of-plane displacement have evidenced the three dimensional nature of cold-expansion process in terms of out-of-plane displacements changing as the angular direction rises from 0° to 180°, and in the lower values observed at the inlet face compared to that at the outlet face, and in the lower values obtained as the plate thickness increases. The FE-experimental comparison has shown a good agreement of the position of the elastic–plastic boundary; the comparison of FE hoop residual stress with Guo's solution has also evidenced a substantial agreement. On the other hand the comparison of experimental and analytical results has shown that the predicted peak of the out-of-plane displacement was close to that measured despite the differences in the plastic radius position.

As a result, the proposed coupled approach (experimental measurement of displacement and following optimization of a FE analysis to get the same experimental field of out-of-plane displacements) benefits both of the accuracy and faithful observation of the results of the split-sleeve cold-working process and of the flexible tools of FE analysis to calculate residual stresses. By means of the knowledge of the residual stresses it is then well established how to predict fatigue life of the expanded hole. Therefore, the proposed methodology is quite versatile and can also be proposed as quality-control technique in the manufacturing processes of cold-expanded holes.

Appendix

In the plastic domain, the closed-form solution for both radial and circumferential stresses was found in terms of $\alpha_{(r)}$ Budiansky's parameter [21]:

$$\sigma_{r(r)} = \sigma_{(r)} \sqrt{\frac{1+R}{2}} \left(\cos \alpha_{(r)} - \frac{1}{\sqrt{1+2R}} \sin \alpha_{(r)} \right) \quad (7a)$$

$$\sigma_{\theta(r)} = \sigma_{(r)} \sqrt{\frac{1+R}{2}} \left(\cos \alpha_{(r)} + \frac{1}{\sqrt{1+2R}} \sin \alpha_{(r)} \right) \quad (7b)$$

In equations (7a) and (7b) the $\sigma_{(r)}$ is the effective stress during the loading step, where $\sigma_{(r)} = \sigma_y$ results at elastic–plastic boundary. The effective stress is defined in terms of

the J_2 deformation theory of plasticity and the yield criterion, and can be expressed in terms of $\alpha_{(r)}$ Budiansky's parameter by the following expression:

$$\frac{\sigma_{(r)}}{\sigma_y} = \left(\frac{a_1 \sin \alpha_p + a_2 \cos \alpha_p}{a_1 \sin \alpha + a_2 \cos \alpha}\right)^{\mu} \exp\left(\frac{2a_1(1+R)(\alpha - \alpha_p)}{a_1^2 + a_2^2}\right)$$

(8)

Where, a_1, a_2, and μ parameters depend on the strain-hardening exponent, n, and the level of plastic anisotropy, R.

The $\sin(\alpha_{(r)})$ and $\cos(\alpha_{(r)})$ terms can be found by combining the solutions of elastic and plastic stresses under the condition $\alpha = \alpha_p$ and $\sigma_{(r)} = \sigma_y$ at $r = r_p$:

$$\sin \alpha_p = \sqrt{1+2R}\left(\frac{b}{r_p}\right)^2 \left[(1+2R)\left(\frac{b}{r_p}\right)^4 + 1\right]^{-0.5}$$

(9a)

$$\cos \alpha_p = \left[(1+2R)\left(\frac{b}{r_p}\right)^4 + 1\right]^{-0.5}$$

(9b)

If the plate undergoes plastic deformation, the residual radial displacement of the plate, $u_{(a)}$ at $r = \alpha$ is derived from equations (2) and (7a) under condition of stress equilibrium:

$$u_{(a)} = \frac{a\sigma_y}{E}\sqrt{\frac{1+R}{2}}\left[(1-\lambda)\cos \alpha_a + \frac{1+\lambda}{\sqrt{1+2R}}\sin \alpha_a\right]$$

$$\times \left\{\left(\frac{a_1 \sin \alpha_p + a_2 \cos \alpha_p}{a_1 \sin \alpha_a + a_2 \cos \alpha_a}\right)^{\mu} \exp\left[\frac{2a_1(1+R)(\alpha_a - \alpha_p)}{a_1^2 + a_2^2}\right]\right\}^{n}$$

(10)

The relationship between r_p, α_a, and α_p can be obtained from equations (2) and (9a) and stress equilibrium equation at elastic–plastic boundary $r = r_p$:

$$\frac{r_p}{a} = \sqrt{\frac{\sin \alpha_a}{\sin \alpha_p}}\left(\frac{a_1 \sin \alpha_p + a_2 \cos \alpha_p}{a_1 \sin \alpha_a + a_2 \cos \alpha_a}\right)^{\gamma}$$

(11)

$$\exp\left[\frac{(n^2 - 1)\sqrt{(1+2R)}(\alpha_a - \alpha_p)}{2(n^2 + 1 + 2R)}\right]$$

Thus, r_p, α_a, α_p can be solved from equations (9), (10) and (11). With these parameters known, the radial and circumferential stresses at any point in the plastic domain can be obtained from equations (7a) and (7b) with the aid of equation (8).

The out-of-plane displacements shown in equation (6) can be derived in term of Budiansky's parameter by combining equations (7) and (8):

$$v_{z(r)} = \int_a^{r_p} \left(\frac{1}{E_s} - \frac{1}{E}\right)\left[2\sigma_{(r)}\sqrt{\frac{1+R}{2}}\cos \alpha_{(r)}\left(1 - \frac{R}{1+R}\right)\right] dz_{(r)}$$

(12)

Given the complex form of the equations (7b) and (8), the solution of out-of-plane displacement, $v_{z(r)}$, cannot be readily solved by integrating equations (12). Therefore, an approach based on Riemann's integral was adopted to partition the plastic domain $[a, r_p]$ into i sub-intervals $[r_{i-1}, r_i]$. The value of $v_{z(r)}$ in the corresponding interval is approximated by the area in the i sub-interval and the resulting area sum will converge to the exact solution of $v_{z(r)}$ as the i sub-interval size tends to zero. In this analysis, the step of the i sub-interval was 0.72 mm for a total number of 15 steps.

References

1. FTI Process Specification 8101D (1994) Cold expansion of holes using the standard split sleeve system and countersink cold expansion. Fatigue Technology Inc. (www.fatiguetech.com)
2. Stefanescu D, Edwards L, Fitzpatrick ME (2002) X-ray diffraction measurement of residual stresses surrounding a cold expanded hole. Mater Sci Forum 404–407:185–190
3. Nadai A (1943) Theory of the expanding of boiler and condenser tube joints through rolling. Trans ASME 65:865–880
4. Guo W (1993) Elastic–plastic analysis of a finite sheet with a cold-worked hole. Eng Fract Mech 46:465–472
5. Hsu YC, Forman RG (1975) Elastic–plastic analysis of an infinite sheet having a circular hole under pressure. J Appl Mech 42:347–352
6. Rich DL, Impellizzeri LF (1977) Fatigue analysis of cold-worked and interference fit fastener holes, cyclic stress–strain and plastic deformation aspects of fatigue crack growth. ASTM STP 637:153–175
7. Ball DL (1995) Elastic–plastic stress analysis of cold expanded fastener holes. Fat Frac Eng Mat Struct 18:47–63
8. Pasta S (2007) Fatigue crack propagation from a cold-worked hole. Eng Fract Mech 74:1525–1538
9. Pavier MJ, Poussard GC, Smith DJ (1985) A finite element simulation of the cold-expansion process for fastener holes. J Strain Anal 32(4):287–300
10. Pavier MJ, Poussard GC, Smith DJ (1998) Finite element modeling of the interaction of residual stress with mechanical load for a crack emanating from a cold worked fastener hole. J Strain Anal 33(4):275–289
11. de Matos PFP, Moreira PMGP, Camanho PP, de Castro PMST (2005) Numerical simulation of cold working of rivet holes. Finite Elem Anal Des 41:989–1007
12. Nigrelli V, Pasta S (2008) Finite-element simulation of residual stress induced by split-sleeve cold-expansion process of holes. J Mat Proc Tech 205:290–296
13. Ozdemir AT, Edwards L (1996) Measurements of the three-dimensional residual stress distribution around split-sleeve cold-expanded holes. J Strain Anal 31(6):413–421
14. Zhang Y, Fitzpatrick ME, Edwards L (2002) Measurement of the residual stresses around a cold expanded hole in an EN8 steel plate using the contour method. Mat Sci For 404–407:527–534
15. Prime MB, Sebring RJ, Edwards JM, Hughes DJ, Webster PJ (2004) Laser surface-contouring and spline data-smoothing for residual stress measurement. Exp Mech 44(2):176–184
16. Priest M, Poussard CG, Pavier MJ, Smith DJ (1995) An assessment of residual-stress measurements around cold-worked holes. Exp Mech 35(4):361–366

17. Pina JCP, Dias AM, de Matos PFP, Moreira PMGP, de Castro PMST (2005) Residual stress analysis near a cold expanded hole in a texture Alclad sheet using X-ray diffraction. Exp Mech 45 (1):83–88

18. Stefanescu D, Steuwer A, Owen RA, Nadri B, Edwards L, Fitzpatrick ME, Withers PJ (2004) Elastic strains around cracked cold-expanded fastener holes measured using the synchrotron X-ray diffraction technique. J Strain Anal 39(5): 459–469

19. Stefanescu D (2003) Experimental study of double cold expansion of holes. J Strain Analysis 38(4):339–347

20. Sanford RJ, Link RE (1989) Holographic measurement of the elastic–plastic boundary surrounding cold-expanded holes. J Strain Anal 24(2):103–106

21. Cirello A, Pasta S (2008) Displacement measurement through digital image correlation and digital speckle pattern interferometry techniques in cold-expanded holes. Strain. doi:10.1111/j.1475-1305.2008.00469.x

22. Poolsuk S, JrWN S (1978) Measurement of the elastic–plastic boundary around coldworked fastener holes. J App Mech Trans ASME 45(3):515–520

23. Mangasarian OL (1960) Stress in the plastic range around a normally loaded circular hole in an infinite sheet. J App Mech 27:65–74

24. Budiansky B (1959) A reassessment of deformation theories of plasticity. J App Mech 81:259–264

25. ASTM (2000) Standard test method for tensile strain-hardening exponents (n-values) of metallic sheet materials. ASTM E 646:607–613

26. COMET5 technical data. Steinbichler Optotechnik, Neubeuern. (http://www.steinbichler.de)

27. VDI/VDE 2634 Part 2: Optical 3D measuring systems—optical systems based on area scanning, VDI/VDE Society of Measuring and Automation Techniques, VDI/VDE guidelines, Düsseldorf, August, 2002

28. Rhinoceros practical guide. Rhinoceros®. (www.rhino3d.com)

29. Jeffrey Fluhrer. DEFORM™ 3D Version 5.03 Design environment for FORMing. Scientific Forming Technologies Corporation 2003

30. Bauschinger J (1881) Civilingenieur 27:289

31. Forcellese A, Fratini L, Gabrielli F, Micari F (1998) The evaluation of springback in 3D stamping and coining processes. J Mater Process Technol 80–81:108–112